Biophysical Journal
Article

Biophysical Society

Antioxidant and Membrane Binding Properties of Serotonin Protect Lipids from Oxidation

Slim Azouzi,[1] Hubert Santuz,[1] Sandrine Morandat,[2] Catia Pereira,[1] Francine Côté,[3] Olivier Hermine,[3] Karim El Kirat,[4] Yves Colin,[1] Caroline Le Van Kim,[1] Catherine Etchebest,[1,*] and Pascal Amireault[1,3,*]

[1]Université Sorbonne Paris Cité, Université Paris Diderot, INSERM, Unité Biologie Intégrée du Globule Rouge UMR-S1134, Institut National de la Transfusion Sanguine, Laboratoire d'Excellence GR-Ex, Paris, France; [2]Sorbonne Universités, Université de Technologie de Compiègne, CNRS, Laboratoire de Génie Enzymatique et Cellulaire FRE 3580, Centre de Recherche Royallieu, Compiègne, France; [3]Université Sorbonne Paris Cité, Université Paris Descartes, INSERM, CNRS, Laboratory of Cellular and Molecular Mechanisms of Hematological Disorders and Therapeutic Implications U1163, Institut Imagine, Laboratoire d'Excellence GR-Ex, Paris, France; and [4]Sorbonne Universités, Université de Technologie de Compiègne, CNRS, Laboratoire de BioMécanique et BioIngénierie UMR 7338, Centre de Recherche Royallieu, Compiègne cedex, France

ABSTRACT Serotonin (5-hydroxytryptamine, 5-HT) is a well-known neurotransmitter that is involved in a growing number of functions in peripheral tissues. Recent studies have shown nonpharmacological functions of 5-HT linked to its chemical properties. Indeed, it was reported that 5-HT may, on the one hand, bind lipid membranes and, on the other hand, protect red blood cells through a mechanism independent of its specific receptors. To better understand these underevaluated properties of 5-HT, we combined biochemical, biophysical, and molecular dynamics simulations approaches to characterize, at the molecular level, the antioxidant capacity of 5-HT and its interaction with lipid membranes. To do so, 5-HT was added to red blood cells and lipid membranes bearing different degrees of unsaturation. Our results demonstrate that 5-HT acts as a potent antioxidant and binds with a superior affinity to lipids with unsaturation on both alkyl chains. We show that 5-HT locates at the hydrophobic-hydrophilic interface, below the glycerol group. This interfacial location is stabilized by hydrogen bonds between the 5-HT hydroxyl group and lipid headgroups and allows 5-HT to intercept reactive oxygen species, preventing membrane oxidation. Experimental and molecular dynamics simulations using membrane enriched with oxidized lipids converge to further reveal that 5-HT contributes to the termination of lipid peroxidation by direct interaction with active groups of these lipids and could also contribute to limit the production of new radicals. Taken together, our results identify 5-HT as a potent inhibitor of lipid peroxidation and offer a different perspective on the role of this pleiotropic molecule.

INTRODUCTION

Oxidation of cellular components such as DNA, proteins, or lipids is associated with a number of physiopathological situations and degenerative diseases (1–4). Among those oxidation reactions, lipid peroxidation (LPO) has important cellular consequences because it may alter the permissive barrier function of the membrane and its capacity to harbor a regulated signaling platform (5,6). For example, many groups have shown that oxidized lipids can promote amyloid formation (7–9), and for a more complete review, please see Kinnunen et al. (10) and Volinsky and Kinnunen (11). Lipid peroxidation results from the interaction of reactive oxygen species (ROS) with unsaturated bonds of lipids and involves three main phases, i.e., initiation, propagation, and termination (Fig. S1) (12,13). During the initiation step, a hydrogen atom is abstracted from a polyunsaturated fatty acid (PUFA) (Scheme S1, *reaction 1*) (14,15). The resulting alkyl radical reacts with oxygen to form a peroxyl radical (LOO•) (Scheme S1, *reaction 2*). This radical can then abstract hydrogen from another unsaturated fatty acid, producing a lipid hydroperoxide and a new alkyl radical (Scheme S1, *reaction 3*). The chain reaction can propagate in the membrane and will terminate when two radicals react (Scheme S1, *reaction 5*) or when it encounters an antioxidant. Actually, aside from this simplistic description, reaction products can be extremely diverse, with different rates of formation and half-life, and depend on the lipid structure. Understanding of the mechanisms of action of antioxidants is difficult and makes the design of potent molecules complex (3). As such, study of the particular

Submitted November 10, 2016, and accepted for publication March 30, 2017.

*Correspondence: catherine.etchebest@inserm.fr or pamireault@ints.fr

Slim Azouzi and Hubert Santuz contributed equally to this work.

Editor: Arne Gericke.

http://dx.doi.org/10.1016/j.bpj.2017.03.037

properties of vitamin C and vitamin E, two natural antioxidants, is informative. Vitamin E, particularly α-tocopherol, a lipid-soluble antioxidant found in polyunsaturated phospholipid-rich domains (16) can both intercept free radicals and terminate lipid oxidation by adapting its position inside the membrane regarding the composition of the latter (17). Vitamin C, a water-soluble antioxidant, has been shown to scavenge free radicals in aqueous phases and can regenerate α-tocopherol (18). These two examples illustrate the fact that both its localization and its capacity to react with and stabilize radicals are important properties of an antioxidant to evaluate its potency in a cellular context.

Melatonin, an hormone synthetized from serotonin (5-HT), has pharmacological properties that regulate important functions (19) and is additionally recognized as a natural antioxidant (20–24). Its antioxidant capacity lies in the indole moiety of the molecule, which can scavenge different type of radicals (hydroxyl, alkoxyl, and peroxyl) (20). Surprisingly, even though 5-HT shares the indole nucleus with Mel (Fig. 1), it has received less attention as an antioxidant molecule, and its antioxidative properties remain less documented. However, some studies suggest a greater potency of 5-HT, when compared to other antioxidants, to inhibit membrane peroxidation in different cell types (22,25–27).

Yet, the importance and ubiquity of this molecule is illustrated by its involvement in a wide array of brain functions (28), and in a growing number of functions in peripheral organs such as gut, pancreas, liver, mammary gland, and heart (29).

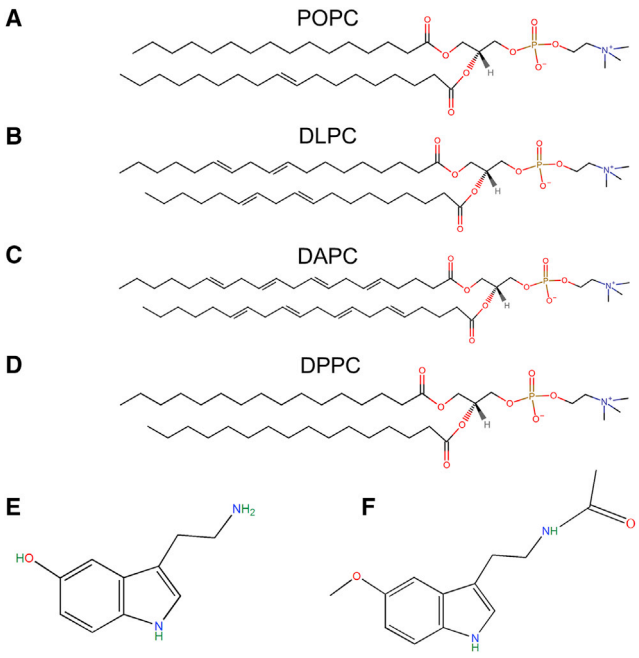

FIGURE 1 Chemical structure of lipids and molecules used. (*A*) POPC, (*B*) DLPC, (*C*) DAPC, (*D*) DPPC, (*E*) Serotonin, (*F*) Melatonin. To see this figure in color, go online.

Among those, it was recently shown that 5-HT plays a pivotal role in the survival of red blood cells (RBCs) in vivo (30). Unexpectedly, addition of 5-HT to mature RBCs stored in vitro, retarded hemolysis during storage and prolonged their life span after transfusion (31). No 5-HT receptors were detected at the RBC surface, suggesting that 5-HT's protecting role lies in a non-receptor-mediated action, i.e., by acting as an antioxidant. Protective mechanisms of 5 HT are difficult to resolve in vivo, insofar as a large variety of molecules with different reactivity properties are present. Interestingly, a recent study exposes that 5-HT is able to interact with lipid membranes (32), a property that can be related to the nonspecific function of 5-HT observed in RBCs.

Together, these findings prompted us to characterize the mechanisms by which 5-HT exerts its antioxidant properties. We hypothesized that the 5-HT protective effect on RBC is mediated both by its antioxidant properties and its capacity to interact with lipid bilayers, leading to an effective protection against lipid peroxidation. Hence, we developed an interdisciplinary approach combining biochemical, biophysical, and molecular dynamics (MD) simulations techniques to characterize the antioxidant capacity of 5-HT in relation to its interaction with lipid membranes with diverse degrees of unsaturation in lipid alkyl chains. In addition, we investigated the 5-HT protective effect on membrane oxidized by two different oxidant agents.

Our data clearly indicate that the 5-HT antioxidant activity is preferentially located at the interface between polar headgroups and glycerol moiety of lipids. Importantly, we observe that changes in interaction between 5-HT and the alkyl chains depend on the unsaturation degree of lipids. Moreover, we notice significant differences in the 5-HT antioxidant effect depending on the source of oxidation tested. On these bases, we propose an original mechanism that accounts for the 5-HT capacity in protecting membranes from oxidative stress. Due to its special location, 5-HT can intercept the diffusion of ROS species and intervene along the propagation and termination of LPO by interacting with oxidized lipids. Importantly, these results contribute to a better understanding of the potential antioxidant effect of 5-HT on RBC in vivo.

MATERIALS AND METHODS

Materials

Serotonin hydrochloride (5-HT), melatonin (Mel), 1,2-dilinoleoyl-*sn*-glycero-3-phosphocholine (DLPC, 18:2−18:2 PC), 1,2-Diarachidonoyl-*sn*-glycero-3-phosphocholine (DAPC, 20:4−20:4 PC), 1-palmitoyl-2-oleoyl-*sn*-glycero-3-phosphocholine (POPC, 16:0−18:1 PC), 1,2-dipalmitoyl-*sn*-glycerol-3 phosphocholine (DPPC, 16:0–16:0 PC), 2,2-azo-bis(2-methylamidinopropane) dihydrochloride (AAPH), 4-(2-Hydroxyethyl) piperazine-1-ethanesulfonic acid (HEPES), and cumene hydroperoxide (CumOOH) were purchased from Sigma-Aldrich (St. Louis, MO). 6-dodecanoyl-2-dimethylaminonaphtalene (Laurdan) and 4,4-Difluoro-5-(4-phenyl-1,3-butadienyl)-4-bora-3a,

4a-diaza-s-indacene-3-undecanoic acid (BODIPY 581/591 C11) were obtained from molecular probes. [3H] 5-HT (75.8 Ci/mmol) was purchased from PerkinElmer (Waltham, MA).

RBC Samples

Healthy blood samples were obtained from the National Institute for Blood Transfusion (Paris, France). RBC samples were washed three times with phosphate-buffered saline (PBS: 137 mM NaCl, 2.6 mM KCl, 8.1 mM Na2HPO4, 1.47 mM KH2PO4 pH 7.4) before experiments.

Flow Cytometry and Confocal Microscopy

Antioxidant activity of 5-HT in RBC membranes was evaluated as described by Fu et al. (33). Briefly, 25 nmol of BODIPY 581/591 C11 was incubated with 10^{10} RBC at 37°C for 30 min in PBS. FACSCanto II (BD Biosciences, San Jose, CA) with a 488-nm excitation laser was used for flow cytometry measurements. The green and red fluorescence intensities of each event were measured using 530- (30-nm band-pass) and 585-nm (42-nm band-pass) filters, respectively. For microscopy analysis, RBC samples were placed between slide and coverslip and observed on an inverted LSM 700 confocal laser scanning microscope (Carl Zeiss, Oberkochen, Germany) equipped with a 100× oil immersion objective.

RBC Oxidation

A 2% suspension of RBC in PBS was incubated with CumOOH at room temperature in the presence of indole compounds. Concentration of CumOOH was of 150 and 250 μM for lipid peroxidation and oxidative hemolysis experiments, respectively.

Preparation of Liposomes

Phospholipids alone or phospholipids/indole compounds mixtures were dried under a nitrogen stream and then kept under high vacuum for 2 h to obtain a solvent-free film. The dry film was then dispersed in HEPES buffer (10 mM HEPES, 150 mM NaCl pH 7.4) to produce multilamellar vesicles (MLVs). To prepare large unilamellar vesicles (LUVs), MLVs were extruded 19 times through 200-nm nucleopore polycarbonate membrane filters using a syringe-type extruder (Avanti Polar Lipids, Alabaster, AL). Small unilamellar vesicles (SUVs) were obtained by sonicating MLVs to clarity (three cycles of 2 min 30 s) using a 500 W titanium probe sonicator while being kept in ice. Then the liposome suspension was filtered on a 0.2 μm Acrodisc (Pall Laboratory, Port Washington, NY) to remove titanium particles. The size of liposomes was determined by dynamic light scattering using a Zetasizer Nano-ZS (Malvern Instruments, Malvern, UK) (Table S1). The range of polydispersity index for all the SUVs was [0.05–0.15].

Laurdan Fluorescence

Generalized polarization (GP) of Laurdan probe was determined in SUVs of POPC, DPPC, or DLPC alone or with 1, 5, and 10 mol % of 5-HT. Laurdan was added to preformed SUVs at a molar ratio of 110:1 (lipid/Laurdan). Laurdan was excited at 360 nm and fluorescence emission intensities at 435 and 490 nm were measured at 37°C using a Varian Cary Eclipse fluorescence spectrophotometer (Agilent Technologies, Danbury, CT) and the GP values were calculated as described in Fadel et al. (34).

Binding of 5-HT to Lipid Membranes

Various concentrations of unlabeled 5-HT were added to a solution of LUVs at a final concentration of 0.1 mM in HEPES buffer containing 1.3 nM [^{3}H] 5-HT as a radioactive tracer. After incubation for 30 min at 37°C, the mixture was centrifuged at 100,000 × g for 60 min at 4°C with an Airfuge Air-Driven Ultracentrifuge (Beckman Coulter, Pasadena, CA). Pellets were suspended with 200 μL of ethanol and then added to a liquid scintillation counter. The amount of 5-HT binding was determined by measuring the retained radioactivity in the lipid fraction. Uptake of 5-HT by RBC membranes was determined by the inhibitor-oil stop method as described in Jarvis et al. (35). Experimental points were fitted with a Langmuir equation to determine the theoretical saturation of the lipid membrane with 5-HT molecules. The Langmuir equation used was as follows:

$$A = A_{\max} \times \frac{X}{(K_d + X)},$$

where A is the 5-HT/lipid molar ratio.

This fit of the data points permitted us to determine the maximum 5-HT/lipid molar ratio $A_{\max}$ and K_d, the dissociation constant.

UV/visible Spectroscopy

Antioxidant activity of 5-HT and Mel in liposomes was assessed by measuring the amount of conjugated dienes using UV/visible spectroscopy. DLPC SUVs containing 1.5 mol % 5-HT or Mel prepared in HEPES buffer were mixed with 2 mM of AAPH, the peroxyl radical oxidizing agent, to reach a final lipid concentration of 0.1 mg/mL. For external oxidation conditions, Fenton reagents (0.15 mM of $FeSO_4$ and 0.6 mM of H_2O_2) were added to the liposome dispersion immediately before data collection. The oxidation was monitored with a Varian Cary Eclipse UV/visible spectrophotometer at 37°C.

The percentage of lipid peroxidation was calculated using the following equation:

$$\%_{\text{Peroxidation}} = \frac{DO^{230\ \text{nm}}[\text{Sample}_{t=180\ \text{min}}] - DO^{230\ \text{nm}}[\text{Sample}_{t=0\ \text{min}}]}{DO^{230\ \text{nm}}[\text{Control}_{t=180\ \text{min}}] - DO^{230\ \text{nm}}[\text{Control}_{t=0\ \text{min}}]} \times 100,$$

where *Control* corresponds to lipid without 5-HT and Mel.

Simulations

MD simulations were carried out on lipid membrane with different degrees of unsaturation (POPC, DLPC, and DAPC), in presence or absence of 5-HT. A DLPC bilayer containing 10% of oxidized lipids was also simulated. Three types of DLPC oxidized products were studied: two with an additional peroxyl group ($Pl^{\bullet}$) either at position 9 or at position 13 of the linoleic acid chain (Z,E-9- $Pl^{\bullet}$ and Z,E-13- $Pl^{\bullet}$), and one with an hydroperoxide (Hpd) group at position 13 of the linoleic acid chain

(Z,E-13-HPd). The simulated bilayers consisted of 128 phospholipid molecules (64 by leaflet) and were fully hydrated with ~40 water molecules per lipid. The starting structure for POPC was taken from previous reports (36–38). The DLPC bilayer was constructed from a SLPC bilayer obtained by CHARMM-GUI interface (www.charmm-gui.org) (39). Starting structure for DAPC was constructed with the CHARMM-GUI interface (39). All simulations were performed for 150 ns to obtain equilibrated membranes. Classical membrane properties, i.e., accessible surface area of lipid headgroups, membrane thickness, and density profiles, were controlled and correlated with experimental data. Details are given in Table S3. An equilibrated DLPC was used as the starting structure for the oxidized bilayers. Then, to account for ~10% oxidation, 12 lipids were manually converted in oxidized ones (six per leaflet) and simulated for 150 ns to obtain equilibrated membranes.

For simulations with 5-HT, endpoint conformations of previous simulations were used as a starting point. Only the charged form of 5-HT was considered because the pKa of its amino group is 9.97. For each system, six molecules of 5-HT were added to the system and placed in the water phase with three molecules equally distant per compartment. Water molecules within 0.6 nm of the center of mass of 5-HT were removed with a home-made script. To neutralize the system, six water molecules were randomly picked and replaced by a chloride ion.

Force field parameters for 5-HT were taken from Shan et al. (40) and use the CHARMM27 (GROMACS; http://www.gromacs.org/) force field. For lipids, the CHARMM36 lipid force field (41) was used with optimization for PUFA chains (42). Force field topology for GROMACS (www.gromacs.org) was taken from Piggot et al. (43). Parameters of oxidized lipids were taken from Garrec et al. (44) and manually converted into GROMACS format.

MD simulations were performed with the GROMACS package version 4.5.7 (45). All bond lengths were constrained with LINCS (http://www.lincsproject.org/) (46,47). Temperature was maintained at 303 K with the velocity-rescale method (48) and a time constant of 0.2 ps. Pressure was maintained semiisotropically at 1 bar using the Parrinello-Rahman algorithm (49) with a time constant of 1.0 ps. The neighbor list was updated every 10 steps with a cutoff of 1.2 nm. Lennard-Jones interactions were switched to zero between 0.8 and 1.2 nm. Particle mesh Ewald (50) with real space cutoff at 1.2 nm was used for electrostatics. After minimization, systems were equilibrated for a 1-ns period, and then simulated during 400 ns (production time). Analyses were performed on the last 350 ns.

The potential of mean force (PMF) of one molecule of 5-HT crossing the bilayer was obtained using umbrella sampling simulations and by applying the weighted histogram analysis method (WHAM) (51) as implemented in the software g_wham (52). More details on the protocol can be found in the Supporting Material.

RESULTS

Serotonin Prevents Lipid Peroxidation in RBC Membranes

We first used the fluorescent probe BODIPY 581/591 as a sensor of oxidative stress to evaluate the capacity of 5-HT and Mel to protect RBC from an oxidative challenge, i.e., peroxidation due to CumOOH. This probe transfers to RBC membrane and its oxidation leads to an increase in the red/green ratio of the detected fluorescence (33) (Fig. S2), allowing us to obtain quantitative information on the antioxidant activity of 5-HT. CumOOH treatment of BODIPY 581/591-RBC leads to oxidation of the probe that reaches a plateau after 120 min (Fig. 2 *A*, *solid dots*). Probe oxidation is dose-dependently inhibited when 5-HT is coincubated with CumOOH, revealing that 5-HT behaves as a powerful antioxidant (Fig. 2 *A*). This inhibition of lipid peroxidation by 5-HT is more clearly illustrated when the peroxidation level is normalized and plotted against the 5-HT concentration (Fig. 2 *B*, *solid uptriangle*) with a calculated IC_{50} of 35.2 ± 1.2 μM. Most interestingly, when RBCs are preincubated with 5-HT, then washed with PBS, before the addition of CumOOH, the antioxidant activity of 5-HT is enhanced when compared with the coincubation condition (Fig. 2 *B*, *solid circle*). In this condition, even though 5-HT was removed from the aqueous phase, the IC_{50} value dropped to 5.5 ± 0.9 μM whereas a concentration of 30 μM is sufficient to reach a maximum inhibitory effect. This suggests that some 5-HT molecules associate with RBCs and are able to prevent probe oxidation. When compared with its well-characterized analog, Mel, our results show that Mel dose-dependently prevents membrane lipid peroxidation (Fig. 2 *C*, *solid uptriangle*) but with an IC_{50} considerably increased (184.4 ± 0.4 μM). Also, in contrast to 5-HT, preincubation, and washing of Mel with lipid membranes before CumOOH addition, severely reduced its antioxidant activity (Fig. 2 *C*, *solid circle*).

This last result suggests that the two indoles operate through different antioxidant mechanisms, despite their

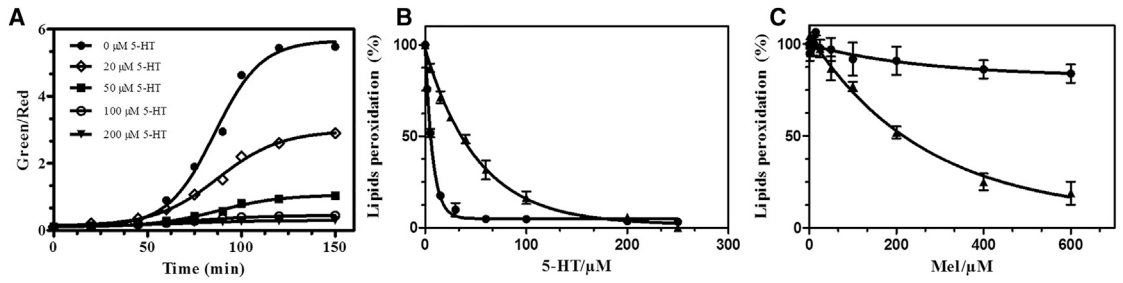

FIGURE 2 5-HT protects RBCs from cumene hydroperoxide-induced oxidation. (*A*) Shown here is the time course of the lipid peroxidation of RBCs labeled with the oxidation-sensitive probe BODIPY 581/591 C11 (BODIPY-RBC). CumOOH (150 μM) and 5-HT were added at $t = 0$ and the green/red fluorescence intensities were measured using flow cytometry. Inhibition of CumOOH-induced lipid peroxidation of BODIPY-RBC by 5-HT (*B*) or Mel (*C*) is given. BODIPY-RBC were preincubated for 30 min and then washed (●) before the CumOOH incubation or coincubated (▲) with the oxidant.

molecular similarities. In the case of Mel, studies have shown that it is able to penetrate lipid bilayers, and even to cross RBC membranes (53), which is not the case for 5-HT (32). As 5-HT is a more potent peroxidation inhibitor in RBC membranes, we next investigated how 5-HT associates with lipid membranes.

Serotonin Interacts with Lipid Bilayers at the Interface

Using a radioactive binding assay, we measured 5-HT binding to RBC membranes. Binding kinetics for 5-HT is characterized by an initial rapid increase, within the first 10 min, followed by a plateau phase indicating saturation (Fig. 3 *A*). Linear correlation between the amount of 5-HT added and the amount of 5-HT bound (Fig. 3 *B*) suggests that 5-HT interacts with the lipid component of RBCs and is consistent with the absence of 5-HT receptors at the RBC surface (31).

RBC membranes are composed of a large variety of lipids. In particular, they are enriched in PUFA (54), which make them more vulnerable to peroxidation. Consequently, the mechanism of the 5-HT antioxidant protective effect was investigated by evaluating its binding to a selection of biomimetic model systems that differ in their alkyl chains degree of unsaturation. We chose 1-Palmitoyl-2-Oleoyl-*sn*-glycero-3-PhosphoCholine (16:0-18:1PC, one unsaturation, POPC) as a model of the RBC membrane composition. Also, to evaluate the impact of the degree of unsaturation on 5-HT binding, we used 1,2-DiLinoleoyl-*sn*-glycero-3-PhosphoCholine (18:2−18:2PC, DLPC) because its oxidized products are well known (21,44) and 1,2-DiArachidonoyl-*sn*-glycero-3-PhosphoCholine (20:4−20:4PC, DAPC) to mimic a highly oxidized-prone bilayer (see Fig. 1 for the chemical structure of the lipids used).

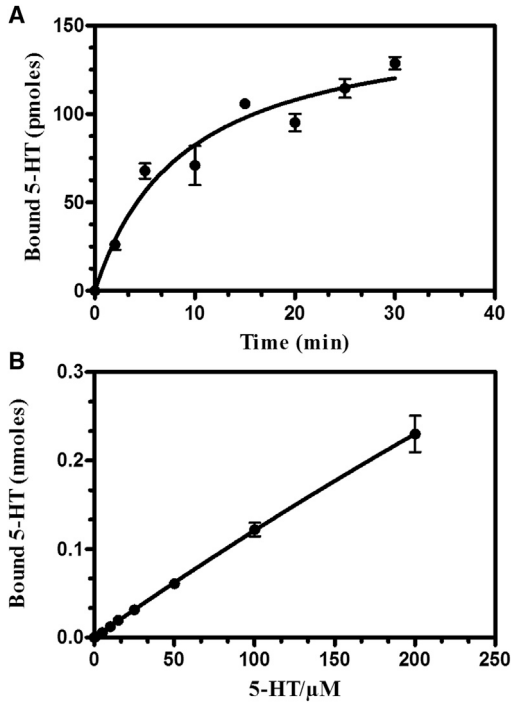

FIGURE 3 Binding of serotonin (5-HT) to RBC membranes. (*A*) Kinetics of 5-HT binding to RBCs is given. (*B*) Linear dose-dependent binding of 5-HT to RBCs is given.

Binding affinity of 5-HT to LUVs of different composition was evaluated and we observed that the 5-HT/lipid molar ratio increases with the amount of 5-HT added (Fig. 4 *A*). The maximum 5-HT/lipid molar ratio equals to 4.21 ± 0.38, 3.24 ± 0.42, and 3.58 ± 0.33 for POPC, DLPC, and DAPC, respectively. The dissociation constant (K_d) for 5-HT binding to lipid membranes calculated from these data equal 647 ± 73 μM, 216 ± 46 μM, and 206 ± 31 μM for POPC, DLPC, and DAPC, respectively (see Materials and Methods). These results reveal that 5-HT binds preferentially to membrane with unsaturated bonds in both alkyl chains while their degree of unsaturation has less impact. These K_d values are similar to those found in a previous study using negatively charged lipids of biological membranes (55). This finding is also in good accordance with a recent work that compared the partitioning coefficient (K_p) of 5-HT into gel and fluid membranes (32). The differences observed with RBC binding may be attributed to the liposomes' size that is considerably smaller than RBC, and/or to a more complex lipid composition of the RBC membrane.

To support our experimental results and obtain atomistic details on the interaction between 5-HT and lipids, we conducted MD simulations of 5-HT with three model membranes composed of the lipids that were tested experimentally (POPC, DLPC, or DAPC). We also evaluated the free energy of 5-HT for crossing the membrane by computing its PMF in those three model membranes (Fig. 4 *B*).

The PMF exhibits negative free energy values in a zone ranging from 1.2 to 3.0 nm from center ($Z = 0$). Energy minima are located at position 2.23 nm ($\Delta G_{min} = -1.88 \pm 0.21$ kcal/mol), 1.91 nm ($\Delta G_{min} = -2.06 \pm 0.17$ kcal/mol), and 1.59 nm ($\Delta G_{min} = -1.93 \pm 0.14$ kcal/mol) for POPC, DLPC, and DAPC, respectively (Fig. 4 *B*). This preferential location of 5-HT at the interface is thus explained by thermodynamics considerations. The free energy minima show a more favorable interaction with DAPC and DLPC compared to POPC, as observed experimentally. These values are also in accordance with the experimental data calculated from K_d values using the equation $\Delta G^\circ = RT\ln K_d$. As expected, a high-energy barrier is calculated when 5-HT is located deeper in the bilayer and reaches a maximum value at the center (ranging from 10 to 15 kcal/mol, depending on the lipid membrane composition of the simulated membrane). This barrier prevents 5-HT molecules from crossing the membrane bilayer on a scalable MD simulation time, but also on an experimental timescale.

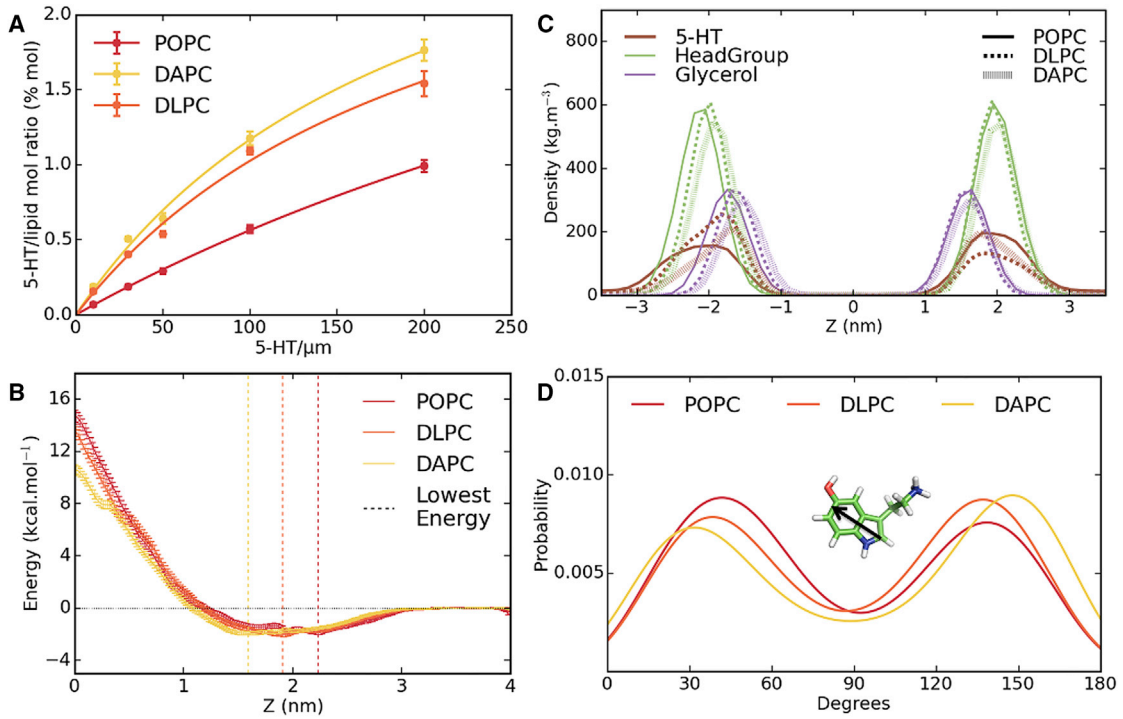

FIGURE 4 Binding, location, and orientation of 5-HT in POPC, DLPC, and DAPC membranes. (*A*) 5-HT binding to different lipid bilayers experimentally is given. (*B*) Shown here is the potential of mean force of 5-HT for POPC, DLPC, and DAPC as a function of the bilayer center. Vertical lines correspond to the minimum energy in each system. (*C*) Mass density profiles for POPC, DLPC, and DAPC, and profiles for the 5-HT, headgroup (Phosphate and Choline), and Glycerol are displayed. (*D*) Shown here is the probability distribution function ($P(\theta)$) of the angle between the indole ring plane and the bilayer normal in each system. To see this figure in color, go online.

Precise location of 5-HT with respect to lipid groups was determined by comparing density profiles of its different chemical groups along the membrane axis (Fig. 4 *C*). 5-HT density profile shows a wide peak, located at 1.8 nm from center in an intermediate position between lipid headgroups (~2.1 nm from center) and the glycerol (1.6 nm from center). Degree of unsaturation does not significantly influence the 5-HT positioning relative to the different lipid groups. Broadness of the 5-HT profile demonstrates its relative mobility at the bilayer interface, which is in relation with negative PMF values in the corresponding zone. These results are in agreement with recent studies describing a similar location of 5-HT in POPC and DOPC membranes (32,56).

To better characterize the 5-HT orientation in the membrane, the angle distributions between the bilayer plane and the indole ring plane were calculated (Fig. 4 *D*) and compared for each type of membrane. Our results show that the indole ring of 5-HT adopts two preferential orientations, i.e., 40° and 130° with respect to the bilayer plane, in agreement with results by Wood et al. (56) for the same form (protonated) of 5-HT in POPC. In addition, our results show a similar angle distribution between DLPC and DAPC membranes. These orientations are in agreement with those deduced by linear dichroism for tryptophan in model lipid membranes, as described by Esbjörner et al. (57), who suggested that indole long-axis points parallel to the membrane plane. NMR measurements (58) also identified maxima at 45° and 135°, even though these maxima were very narrow. Similar orientations were also observed with MD simulations performed on tryptophan-containing peptides (59). Hence, the presence of additional side groups (OH and ammonium groups) does not modify significantly the main orientations of the indole ring. Compared to tryptophan, in which hydrogen bond can be solely established with indole NH group, 5-HT is stabilized by strong additional key electrostatic interactions, i.e., a salt bridge between the 5-HT ammonium group and the phosphate group of lipids.

Besides these strong electrostatic interactions, the mobility of 5-HT is also responsive to competing weaker interactions, i.e., hydrogen bonds between the 5-HT hydroxyl group and polar atoms of lipids or between the 5-HT hydroxyl group and water molecules (Table S2), respectively. It has to be noted that the 5-HT hydroxyl group position that we calculated significantly differs from that observed by Peters et al. (32) in the DOPC bilayer, whatever the protonation state considered.

To go further, we examined in detail the contacts made between 5-HT and the lipid chemical groups (Table 1) of our different model membranes. The majority of 5-HT contacts are, in ranking order, with headgroups, aliphatic chains, and glycerol. Interestingly, we observed a positive

TABLE 1 Contact in Percentage between 5-HT and the Membrane

	Headgroup	Glycerol	Aliphatic Chains
POPC	43.6	22.7	33.7
DLPC	41.2	22.4	36.4
DAPC	38.5	21.2	39.5

Contact was defined by a distance of <0.6 nm between any lipid atoms and the 5-HT center of mass.

correlation between the degree of lipid chain unsaturation and 5-HT contacts with aliphatic chains, because the contact distribution increased from 33.7% for POPC and 36.4% for DPLC to 39.5% for DAPC (Table 1). Accordingly, the number of contacts with headgroups decreases, from 43.6 to 38.5%.

Experimentally, the 5-HT location was evaluated using the Laurdan probe, a fluorescent lipophilic molecule. The GP of Laurdan is sensitive to modification in its polarity environment, which is related to change in accessibilities of water molecules to the membrane hydrophobic core. For the monounsaturated lipid, POPC, 5-HT causes only a slight decrease in GP values (Fig. S3). This result is consistent with a weaker affinity of 5-HT with POPC, in agreement with a position closer to headgroups as identified with MD simulations. For a membrane enriched in PUFA (DLPC), value of the GP increases along 5-HT addition, i.e., the Laurdan environment is changing with increasing 5-HT concentration. This finding is compatible with a deeper location of 5-HT with respect to the membrane, as shown by simulation calculations.

In summary, our in silico and experimental results clearly converge to show that 5-HT associates with lipid membranes, and that the larger the number of unsaturated alkyl bonds, the deeper the location.

Antioxidant Activity of Serotonin Correlates with its Location in the Membrane

How this location might be related to the observed 5-HT protective effect on RBCs remains a main issue. To address this question, we monitored the time evolution of UV absorption from DLPC SUVs undergoing oxidation by hydroxyl radicals (Fenton reaction, Scheme S1, *reactions 6–7*) or by peroxy and alkoxy radicals (AAPH, Scheme S1, *reactions 8–9*) in the presence or absence of 5-HT. The molar percentage of 5-HT chosen was 3.2%, which corresponds to the maximal amount of 5-HT that can bind to DLPC membranes (Fig. 4 *A*).

In the presence of 5-HT, lipid oxidation was reduced by 88% when compared with control liposomes incubated for 3 h in Fenton peroxides (Fig. 5 *A*). In parallel, Mel reduced oxidation by only 48%, showing again that it is less potent than 5-HT in protecting lipids from oxidation. This result contrasts with those obtained by Fukutomi et al. (60), who

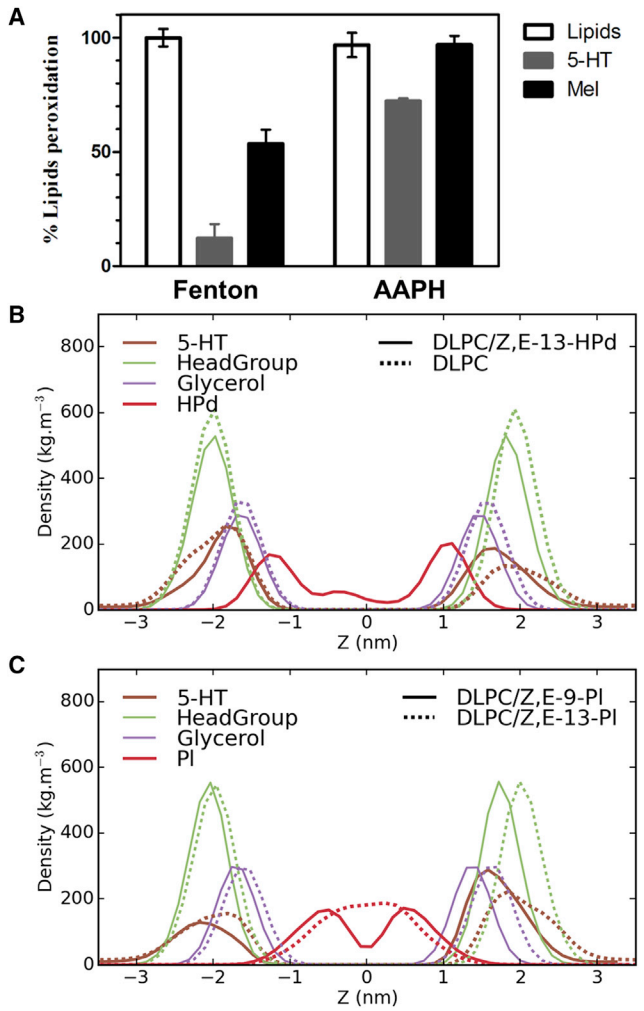

FIGURE 5 Antioxidant activity of 5-HT against different oxidative stress. (*A*) Shown here is the antioxidant activity of membrane-inserted 5-HT against AAPH and $OH^{\bullet}$-induced oxidation in DLPC liposomes. (*B*) Given here are the mass density profiles of DLPC with 10% hydroperoxide-oxidized lipids (Z,E-13-Hpd). (*C*) Shown here are the mass density profiles of DLPC with 10% peroxyl-oxidized lipids (Z,E-13-$Pl^{\bullet}$ and Z,E-9-$Pl^{\bullet}$). Profiles for 5-HT, headgroups (Phosphate and Choline), and Glycerol are displayed along with the oxidized part (Hpd (*B*) or $Pl^{\bullet}$ (*C*)). To see this figure in color, go online.

showed that Mel is more efficient on cisplatin (*cis*-diamine-dichloroplatinum)-induced ROS. This indicates that the nature of the ROS species is a key element in the oxidation-protective effect of Mel and 5-HT (see below).

In experiments with AAPH, 5-HT reduced peroxidation by 18%, showing a weaker antioxidant activity of 5-HT against alkyl and peroxyl radicals. Once again, Mel was less potent than 5-HT in this experiment because it could not prevent, but only delay (Fig. S4), AAPH-induced peroxidation. The indole ring is not affected by the presence of the oxidative agents because no change was observed in its absorbance amplitude.

The differences in 5-HT efficiency with respect to the two oxidative agents can be only attributed to the nature

of chemical products formed along the reactions. Thermolysis of AAPH in solution generates alkyl radicals that react rapidly with oxygen and yield initiating peroxyl radicals (14,15). Then, these radicals can abstract hydrogen from another unsaturated fatty acid and produce a lipid hydroperoxide and a new alkyl radical (12,13). Fenton reaction involves metal ions, which are known to contribute to additional chemical reactions, apart from their initial catalytic role.

Thus, from these data, 5-HT could block the oxidation reaction in two ways. First, its interface localization is compatible with an interposition at the initiation phase of peroxidation by trapping hydroxyl radicals diffusing from bulk water before these radicals interact with unsaturated lipids (LH). Alternatively, its frequent contacts with unsaturated lipid chains suggest it might also interfere during the propagation step. To examine this second hypothesis, we investigated with MD simulations how 5-HT interacts with lipid radicals and per se, how it could contribute to inhibit peroxidation propagation. DLPC bilayer with 10% oxidized lipids were simulated and we focused on three oxidation products of linoleic acid: 13-trans, *cis*-hydroperoxide linoleic acid (Z,E-13-Hpd) containing an Hpd group and involved in propagation and termination steps by leading to the production of aldehydes; 9-*trans*, *cis*-peroxyl linoleic acid (Z-E-9- Pl$^{\bullet}$); and 13-*trans*, *cis*-peroxyl (Z,E-13- Pl$^{\bullet}$)-containing peroxyl (Pl$^{\bullet}$) groups, involved only in the propagation step.

Introduction of an oxidized functional group in the lipid tail leads to modifications of the structural properties of the bilayer (Table S3). The main effect is a decrease in the bilayer thickness. In contrast, distribution of the chemical groups (Hpd, Pl$^{\bullet}$, 5-HT, glycerol, and headgroup), calculated along the membrane normal, is modified (Fig. 5, *B* and *C*) depending on the oxidation state. For membrane enriched with Hpd-oxidized moieties (Fig. 5 *B*), the hydroperoxide group is localized near the lipid's glycerol backbone and 5-HT comes closer to Hpd groups (Fig. 5 *B*). Moreover, the number of contacts between 5-HT and lipid headgroups decreases from 41.2 to 37.3% when compared to pure DLPC (Table S4). This decrease is compensated by an increase in contacts with aliphatic chains (Table S4). These findings can be attributed to 1) a deeper seat of 5-HT and 2) the snorkeling of acyl chains bearing the Hpd group toward the interface where transient hydrogen bonds with water and the polar lipid can be formed.

In the case of peroxyl-containing lipids, Pl-oxidized moieties are found localized inside the bilayer hydrophobic core (Fig. 5 *C*). As already observed by others (44), the oxidized tails do not bend toward the water phase and interdigitation of lipids ends makes Z,E-13-Pl$^{\bullet}$ undistinguishable between the two monolayers. In this last case, the overlap between the distribution of 5-HT and the radical group is very small whereas, interestingly, in the Z,E-9-Pl$^{\bullet}$ membrane, a slight overlap between 5-HT and the Pl$^{\bullet}$ moieties (Fig. 5 *C*) is observed. This behavior may contribute to the weak protective effect observed experimentally. Surprisingly, despite a smaller overlap in distribution with Pl moieties, the number of contacts between 5-HT and alkyl chains is larger for Z,E-13- Pl$^{\bullet}$ compared to Z,E-9- Pl$^{\bullet}$ (Table S4), which would impact further steps of oxidation.

DISCUSSION

In this study, we investigated the antioxidant potential of 5-HT in RBC membranes and in a biomimetic membrane model. In addition, detailed characterization of the interaction between 5-HT and the lipid membrane allowed us to correlate the antioxidant activity of 5-HT and its location in lipid bilayers.

Antioxidant Properties and Molecular Structure of Serotonin

To better understand the functional groups carrying the antioxidant properties of 5-HT, we compared its activity with Mel: an analog with recognized antioxidant properties that also contains an indole structure. Our data show that 5-HT is a more potent antioxidant against lipid peroxidation, in all experimental conditions tested. Comparison of the molecular structure of 5-HT and Mel shows they differ at position 5 of the indole ring: 5-HT comprises a hydroxyl group and Mel a methoxy group (Fig. 1). In addition, Mel has an acyl group attached to its carbon side chain. An earlier investigation by Turjanski et al. (61) considered the relationship between the structure of indole compounds and their antioxidant activity. They examined different chemical reaction pathways of OH$^{\bullet}$ radicals with Mel, 5-HT, and other indole derivatives. Their study revealed that the free-energy changes, obtained by semiempirical quantum calculations in vacuum and in aqueous environment, were similar for all the studied indole derivatives. Hence, they concluded that the 5-methoxy and the N-acetyl groups of Mel are not key functions, in regard to Mel's thermodynamical capacity of ROS trapping (61). Interestingly, among the different derivatives and reaction schemes examined, the favored one involves the formation of a radical from an OH group, which is present in 5-HT and not in Mel.

The role of the hydroxyl group in free radical scavenging was also previously underlined for numerous polyphenols (62–65) and by Fabre et al. (66), who studied lipocarbazole derivatives and their location and orientation in lipid bilayers. Similarly, the study conducted by Álvarez-Diduk et al. (67), who examined N-acetylserotonin ROS scavenging capacity, substantiates the importance of the hydroxyl group. They demonstrated using density functional theory that N-acetylserotonin is more efficient to scavenge HOO$^{\bullet}$ radical than melatonin itself. Despite the differences with this environment, this result offers a valuable explanation for the observations provided in this study. Altogether,

these data highlight the role of the hydroxyl group of 5-HT in ROS scavenging and its probable contribution in the superior capacity of 5-HT to protect against lipid oxidation when compared to Mel.

Serotonin Intercepts ROS at the Lipid/water Interface

Our MD simulation and Laurdan data confirm that 5-HT is located at the membrane interface and deeper within the membrane, depending on the number of unsaturated bonds in alkyl chains. Our binding experiments using radiolabeled 5-HT show that it strongly interacts with lipid bilayers. The 5-HT equilibrated position obtained with MD is between the hydrophobic core and polar surface of lipid bilayers. This preferential interfacial position reflects the amphipathic character of 5-HT having both hydrophobic aromatic rings and hydrophilic NH_3^+ and OH groups. These groups interact with the lipid polar heads, by H-bonding, allowing stabilization of the 5-HT position in the membrane. Recent studies observed a similar location of 5-HT on POPC and DOPC membranes (32,56). Furthermore, the partitioning experiments and energy profiles of 5-HT on DLPC and DAPC bilayers compared to POPC are in favor of a preferential interaction with PUFA-enriched membranes. Also, 5-HT is located slightly deeper in these membranes, which results in a decrease of 5-HT mobility and an increased proximity with hydrophobic chains.

These data indicate that the 5-HT antioxidant activity mainly takes place at the membrane's surface. In this respect, a recent work, studying the location of ROS in membranes, showed that hydroxyl radicals ($OH^\bullet$) accumulate at the interface between headgroups and glycerol group of lipids close to the 5-HT location we observed (68). The author also showed that the $OH^\bullet$ radical forms an H-bond with one of the carbonylester groups of a phospholipid. An H-bond network was established that links $OH^\bullet$ radical to the bulk aqueous solution. The maintenance of this network is a prerequisite for the occurrence of an H-transfer mechanism. Consequently, lipids engaged with 5-HT by hydrogen bonding would be less sensitive to $OH^\bullet$ radicals. Alternatively, when the 5-HT hydroxyl group is hydrogen bonded with water rather than lipid, it will itself be able to capture the radicals as well. Hence, 5-HT is optimally placed to intercept polar oxidizing agents such as hydroxyl radicals. This explains the potent protective effect of 5-HT against hydroxyl radicals produced by the Fenton reaction.

Serotonin Contribution to Lipid Peroxidation Inhibition

This analysis provides an original explanation for the protective effect of 5-HT toward lipid peroxidation: mainly by scavenging ROS before initiating the cascade of reactions involving the lipid molecule itself. Nevertheless, our results clearly show a dependence of 5-HT efficiency with the nature of the lipid alkyl chains, suggesting its direct contribution in the following stages of the LPO as well.

To better understand the mechanism of 5-HT, we compared its antioxidant capacity in two different lipid oxidation reactions, i.e., Fenton reaction and using the free radical initiator AAPH. Although both produce peroxyl radicals, the protective effect of 5-HT clearly differs between the two reactions. This difference could be attributed to different kinetics rates of peroxyl radical production. However, this possibility is unlikely, considering the experiments' timescale and the large difference observed between the 5-HT protective effect in the Fenton and the AAPH condition (88 vs. 18%, respectively). Interestingly, a main difference between these two reactions relies on the presence of a metal ion, the ferrous/ferric ion, in the Fenton reaction. The effect of iron in lipid peroxidation has been studied in several publications (69–72). In the presence of peroxide derivative, it is able to produce new oxyl radicals $LO^\bullet$ or $LOO^\bullet$ (Scheme S1, *reactions 10–11*) from the Hpd group. It can also produce epoxyallylic peroxyl radicals ($OLOO^\bullet$) (12). Even though the formation of lipid to peroxide is a rate-limiting step, it dominates early stages of autoxidation (73) and is a key factor in the propagation stage. Our results clearly show that the interfacial location of 5-HT allows its interaction with the hydroperoxide group of oxidized lipids. Indeed, in contrast to peroxyl, Hpd groups snorkel and spend a fraction of their time in the lipid/water interface, as shown by others (44). Also, hydroperoxides can break down and generate more radical species (74) (Scheme S1, *reaction 4*). Consequently, by interacting with the lipid hydroperoxide reactive group, 5-HT would limit the production of new radicals: a hypothesis fitting with its increased efficiency in the Fenton reaction.

On the other hand, we also show that 5-HT is able to interact, to a lesser extent, with peroxyl radicals. 5-HT could scavenge these radicals, and thus modestly limit the propagation steps involving $LOO^\bullet$. This could explain its weak protective effect observed experimentally in the AAPH reaction.

Taken together, these results allow for a better understanding of the capacity of 5-HT to protect lipid membranes from oxidation. This capacity offers a plausible explanation for the previously observed protective effect of 5-HT on RBCs (31). Indeed, it was demonstrated that 5-HT supplementation decreases the hemolysis of stored RBCs and improves their posttransfusion survival in a mouse model of blood banking. Interestingly, it was shown that lipid oxidation increases, leading to irreversible damages to the membrane and, ultimately, hemolysis during RBC storage in vitro. The decreased 5-HT blood level, in the serotonin-deficient mouse, is associated with a decrease in the plasma antioxidant capacity (30), whereas its normal level, in the lower μM range, suggests that 5-HT might also behave as an antioxidant in vivo.

SUPPORTING MATERIAL

Supporting Material, four figures, four tables, and one scheme are available at http://www.biophysj.org/biophysj/supplemental/S0006-3495(17)30385-5.

AUTHOR CONTRIBUTIONS

S.A., O.H., C.L.V.K., C.E., and P.A. conceived the project. S.A., H.S., F.C., S.M., K.E.K., Y.C., C.E., and P.A. designed the research. S.A., H.S., and C.P. performed experiments. S.M., and K.E.K. contributed analytic tools. S.A., H.S., S.M., C.P., K.E.K., C.E., and P.A. analyzed data. S.A., H.S., Y.C., C.E., and P.A. wrote the paper.

ACKNOWLEDGMENTS

The authors thank Hinde Benjelloun for help with cytometry experiments, and Thierry Peyrard and Eliane Vera at Centre National de Référence pour les Groupes Sanguins (CNRGS) for making available human blood.

S.A. was supported by a Labex GR-Ex Fellowship. The Labex GR-Ex, reference No. ANR-11-LABX-0051 is funded by the program "Investissements d'avenir" of the French National Research Agency, reference No. ANR-11-IDEX-0005-02. H.S. acknowledges the HPC resources granted from GENCI-CINES (grant No. 2014-c2014077209) and computer facilities provided by Region Ile de France and National Institute for Blood Transfusion (SESAME 2009 project). This work was supported by a grant from l'Association Recherche Transfusion (to P.A.).

REFERENCES

1. Sultana, R., M. Perluigi, and D. Allan Butterfield. 2013. Lipid peroxidation triggers neurodegeneration: a redox proteomics view into the Alzheimer disease brain. *Free Radic. Biol. Med.* 62:157–169.
2. Reed, T. T. 2011. Lipid peroxidation and neurodegenerative disease. *Free Radic. Biol. Med.* 51:1302–1319.
3. Kim, G. H., J. E. Kim, …, S. Yoon. 2015. The role of oxidative stress in neurodegenerative diseases. *Exp. Neurobiol.* 24:325–340.
4. Arimon, M., S. Takeda, …, O. Berezovska. 2015. Oxidative stress and lipid peroxidation are upstream of amyloid pathology. *Neurobiol. Dis.* 84:109–119.
5. Ott, M., V. Gogvadze, …, B. Zhivotovsky. 2007. Mitochondria, oxidative stress and cell death. *Apoptosis.* 12:913–922.
6. Ayala, A., M. F. Muñoz, and S. Argüelles. 2014. Lipid peroxidation: production, metabolism, and signaling mechanisms of malondialdehyde and 4-hydroxy-2-nonenal. *Oxid. Med. Cell. Longev.* 2014:360438.
7. Mahalka, A. K., C. P. J. Maury, and P. K. J. Kinnunen. 2011. 1-Palmitoyl-2-(9′-oxononanoyl)-*sn*-glycero-3-phosphocholine, an oxidized phospholipid, accelerates Finnish type familial gelsolin amyloidosis in vitro. *Biochemistry.* 50:4877–4889.
8. Koppaka, V., and P. H. Axelsen. 2000. Accelerated accumulation of amyloid beta proteins on oxidatively damaged lipid membranes. *Biochemistry.* 39:10011–10016.
9. Kinnunen, P. K. J., Y. A. Domanov, …, T. Varis. 2015. Formation of lipid/peptide tubules by IAPP and temporin B on supported lipid membranes. *Soft Matter.* 11:9188–9200.
10. Kinnunen, P. K. J., K. Kaarniranta, and A. K. Mahalka. 2012. Protein-oxidized phospholipid interactions in cellular signaling for cell death: from biophysics to clinical correlations. *Biochim. Biophys. Acta.* 1818:2446–2455.
11. Volinsky, R., and P. K. J. Kinnunen. 2013. Oxidized phosphatidylcholines in membrane-level cellular signaling: from biophysics to physiology and molecular pathology. *FEBS J.* 280:2806–2816.
12. Girotti, A. W. 1998. Lipid hydroperoxide generation, turnover, and effector action in biological systems. *J. Lipid Res.* 39:1529–1542.
13. Yin, H., L. Xu, and N. A. Porter. 2011. Free radical lipid peroxidation: mechanisms and analysis. *Chem. Rev.* 111:5944–5972.
14. Kohri, S., and H. Fujii. 2013. 2,2′-Azobis(isobutyronitrile)-derived alkylperoxyl radical scavenging activity assay of hydrophilic antioxidants by employing EPR spin trap method. *J. Clin. Biochem. Nutr.* 53:134–138.
15. Joshi, G., M. Perluigi, …, D. A. Butterfield. 2006. In vivo protection of synaptosomes by ferulic acid ethyl ester (FAEE) from oxidative stress mediated by 2,2-azobis(2-amidino-propane)dihydrochloride (AAPH) or Fe^{2+}/H_2O_2: insight into mechanisms of neuroprotection and relevance to oxidative stress-related neurodegenerative disorders. *Neurochem. Int.* 48:318–327.
16. Atkinson, J., T. Harroun, …, J. Katsaras. 2010. The location and behavior of α-tocopherol in membranes. *Mol. Nutr. Food Res.* 54:641–651.
17. Marquardt, D., J. A. Williams, …, T. A. Harroun. 2013. Tocopherol activity correlates with its location in a membrane: a new perspective on the antioxidant vitamin E. *J. Am. Chem. Soc.* 135:7523–7533.
18. Bendich, A., L. J. Machlin, …, D. D. M. Wayner. 1986. The antioxidant role of vitamin C. *Adv. Free Radic. Biol. Med.* 2:419–444.
19. Reiter, R. J., D.-X. Tan, and L. Fuentes-Broto. 2010. Melatonin: a multitasking molecule. *Prog. Brain Res.* 181:127–151.
20. Galano, A., D. X. Tan, and R. J. Reiter. 2011. Melatonin as a natural ally against oxidative stress: a physicochemical examination. *J. Pineal Res.* 51:1–16.
21. Tan, D. X., R. J. Reiter, …, R. Hardeland. 2002. Chemical and physical properties and potential mechanisms: melatonin as a broad spectrum antioxidant and free radical scavenger. *Curr. Top. Med. Chem.* 2:181–197.
22. Marshall, K.-A., R. J. Reiter, …, B. Halliwell. 1996. Evaluation of the antioxidant activity of melatonin in vitro. *Free Radic. Biol. Med.* 21:307–315.
23. Galano, A. 2011. On the direct scavenging activity of melatonin towards hydroxyl and a series of peroxyl radicals. *Phys. Chem. Chem. Phys.* 13:7178–7188.
24. García, J. J., L. López-Pingarrón, …, M. Bernal-Pérez. 2014. Protective effects of melatonin in reducing oxidative stress and in preserving the fluidity of biological membranes: a review. *J. Pineal Res.* 56:225–237.
25. Chan, T. Y., and P. L. Tang. 1996. Characterization of the antioxidant effects of melatonin and related indoleamines in vitro. *J. Pineal Res.* 20:187–191.
26. Betten, A., C. Dahlgren, …, K. Hellstrand. 2001. Serotonin protects NK cells against oxidatively induced functional inhibition and apoptosis. *J. Leukoc. Biol.* 70:65–72.
27. Sarikaya, S., and I. Gulcin. 2013. Radical scavenging and antioxidant capacity of serotonin. *Curr. Bioact. Compd.* 9:143–152.
28. Jacobs, B. L., and E. C. Azmitia. 1992. Structure and function of the brain serotonin system. *Physiol. Rev.* 72:165–229.
29. Amireault, P., D. Sibon, and F. Côté. 2013. Life without peripheral serotonin: insights from tryptophan hydroxylase 1 knockout mice reveal the existence of paracrine/autocrine serotonergic networks. *ACS Chem. Neurosci.* 4:64–71.
30. Amireault, P., S. Hatia, …, F. Côté. 2011. Ineffective erythropoiesis with reduced red blood cell survival in serotonin-deficient mice. *Proc. Natl. Acad. Sci. USA.* 108:13141–13146.
31. Amireault, P., E. Bayard, …, F. Côté. 2013. Serotonin is a key factor for mouse red blood cell survival. *PLoS One.* 8:e83010.
32. Peters, G. H., C. Wang, …, P. Westh. 2013. Binding of serotonin to lipid membranes. *J. Am. Chem. Soc.* 135:2164–2171.
33. Fu, Y., N. Klonis, …, L. Tilley. 2009. A phosphatidylcholine-BODIPY 581/591 conjugate allows mapping of oxidative stress in *P. falciparum*-infected erythrocytes. *Cytometry A.* 75:390–404.

34. Fadel, O., K. El Kirat, and S. Morandat. 2011. The natural antioxidant rosmarinic acid spontaneously penetrates membranes to inhibit lipid peroxidation in situ. *Biochim. Biophys. Acta.* 1808:2973–2980.

35. Jarvis, S. M., J. A. Thorn, and P. Glue. 1998. Ribavirin uptake by human erythrocytes and the involvement of nitrobenzylthioinosine-sensitive (*es*)-nucleoside transporters. *Br. J. Pharmacol.* 123:1587–1592.

36. Jämbeck, J. P. M., and A. P. Lyubartsev. Computer simulations of heterogenous biomembranes with the Slipids force field. http://www.fos.su.se/~sasha/SLipids/Downloads.html.

37. Jämbeck, J. P. M., and A. P. Lyubartsev. 2012. Derivation and systematic validation of a refined all-atom force field for phosphatidylcholine lipids. *J. Phys. Chem. B.* 116:3164–3179.

38. Jämbeck, J. P. M., and A. P. Lyubartsev. 2012. An extension and further validation of an all-atomistic force field for biological membranes. *J. Chem. Theory Comput.* 8:2938–2948.

39. Jo, S., T. Kim, …, W. Im. 2008. CHARMM-GUI: a web-based graphical user interface for CHARMM. *J. Comput. Chem.* 29:1859–1865.

40. Shan, J., G. Khelashvili, …, H. Weinstein. 2012. Ligand-dependent conformations and dynamics of the serotonin 5-HT(2A) receptor determine its activation and membrane-driven oligomerization properties. *PLoS Comput. Biol.* 8:e1002473.

41. Klauda, J. B., R. M. Venable, …, R. W. Pastor. 2010. Update of the CHARMM all-atom additive force field for lipids: validation on six lipid types. *J. Phys. Chem. B.* 114:7830–7843.

42. Klauda, J. B., V. Monje, …, W. Im. 2012. Improving the CHARMM force field for polyunsaturated fatty acid chains. *J. Phys. Chem. B.* 116:9424–9431.

43. Piggot, T. J., Á. Piñeiro, and S. Khalid. 2012. Molecular dynamics simulations of phosphatidylcholine membranes: a comparative force field study. *J. Chem. Theory Comput.* 8:4593–4609.

44. Garrec, J., A. Monari, …, M. Tarek. 2014. Lipid peroxidation in membranes: the peroxyl radical does not "float". *J. Phys. Chem. Lett.* 5:1653–1658.

45. Pronk, S., S. Páll, …, E. Lindahl. 2013. GROMACS 4.5: a high-throughput and highly parallel open source molecular simulation toolkit. *Bioinformatics.* 29:845–854.

46. Hess, B., H. Bekker, …, J. G. E. M. Fraaije. 1997. LINCS: a linear constraint solver for molecular simulations. *J. Comput. Chem.* 18:1463–1472.

47. Hess, B. 2008. P-LINCS: a parallel linear constraint solver for molecular simulation. *J. Chem. Theory Comput.* 4:116–122.

48. Bussi, G., D. Donadio, and M. Parrinello. 2007. Canonical sampling through velocity rescaling. *J. Chem. Phys.* 126:014101.

49. Parrinello, M. 1981. Polymorphic transitions in single crystals: a new molecular dynamics method. *J. Appl. Phys.* 52:7182.

50. Essmann, U., L. Perera, …, L. G. Pedersen. 1995. A smooth particle mesh Ewald method. *J. Chem. Phys.* 103:8577.

51. Kumar, S., J. M. Rosenberg, …, P. A. Kollman. 1992. THE weighted histogram analysis method for free-energy calculations on biomolecules. I. The method. *J. Comput. Chem.* 13:1011–1021.

52. Hub, J. S., B. L. de Groot, and D. van der Spoel. 2010. g_wham—a free weighted histogram analysis implementation including robust error and autocorrelation estimates. *J. Chem. Theory Comput.* 6:3713–3720.

53. Tesoriere, L., D. D'Arpa, …, M. A. Livrea. 1999. Melatonin protects human red blood cells from oxidative hemolysis: new insights into the radical-scavenging activity. *J. Pineal Res.* 27:95–105.

54. Koehrer, P., S. Saab, …, N. Acar. 2014. Erythrocyte phospholipid and polyunsaturated fatty acid composition in diabetic retinopathy. *PLoS One.* 9:e106912.

55. Johnson, D. A., S. C. Merlone, …, G. L. Ellman. 1978. Binding of 5-hydroxytryptamine to acidic lipids in an aqueous medium. *J. Neurochem.* 31:713–717.

56. Wood, I., M. F. Martini, and M. Pickholz. 2013. Similarities and differences of serotonin and its precursors in their interactions with model membranes studied by molecular dynamics simulation. *J. Mol. Struct.* 1045:124–130.

57. Esbjörner, E. K., C. E. B. Caesar, …, B. Nordén. 2007. Tryptophan orientation in model lipid membranes. *Biochem. Biophys. Res. Commun.* 361:645–650.

58. Gaede, H. C., W.-M. Yau, and K. Gawrisch. 2005. Electrostatic contributions to indole-lipid interactions. *J. Phys. Chem. B.* 109:13014–13023.

59. de Jesus, A. J., and T. W. Allen. 2013. The role of tryptophan side chains in membrane protein anchoring and hydrophobic mismatch. *Biochim. Biophys. Acta.* 1828:864–876.

60. Fukutomi, J., A. Fukuda, …, M. Yoshida. 2006. Scavenging activity of indole compounds against cisplatin-induced reactive oxygen species. *Life Sci.* 80:254–257.

61. Turjanski, A. G., R. E. Rosenstein, and D. A. Estrin. 1998. Reactions of melatonin and related indoles with free radicals: a computational study. *J. Med. Chem.* 41:3684–3689.

62. Trouillas, P., P. Marsal, …, J.-L. Duroux. 2006. A DFT study of the reactivity of OH groups in quercetin and taxifolin antioxidants: the specificity of the 3-OH site. *Food Chem.* 97:679–688.

63. Anouar, E., P. Kosinová, …, P. Trouillas. 2009. New aspects of the antioxidant properties of phenolic acids: a combined theoretical and experimental approach. *Phys. Chem. Chem. Phys.* 11:7659–7668.

64. Di Meo, F., V. Lemaur, …, P. Trouillas. 2013. Free radical scavenging by natural polyphenols: atom versus electron transfer. *J. Phys. Chem. A.* 117:2082–2092.

65. Fabre, G., I. Bayach, …, P. Trouillas. 2015. Synergism of antioxidant action of vitamins E, C and quercetin is related to formation of molecular associations in biomembranes. *Chem. Commun. (Camb.).* 51:7713–7716.

66. Fabre, G., A. Hänchen, …, P. Trouillas. 2015. Lipocarbazole, an efficient lipid peroxidation inhibitor anchored in the membrane. *Bioorg. Med. Chem.* 23:4866–4870.

67. Álvarez-Diduk, R., A. Galano, …, R. J. Reiter. 2015. N-acetylserotonin and 6-hydroxymelatonin against oxidative stress: implications for the overall protection exerted by melatonin. *J. Phys. Chem. B.* 119:8535–8543.

68. Cordeiro, R. M. 2014. Reactive oxygen species at phospholipid bilayers: distribution, mobility and permeation. *Biochim. Biophys. Acta.* 1838 (1 pt. B):438–444.

69. Tadolini, B., and G. Hakim. 1996. The mechanism of iron (III) stimulation of lipid peroxidation. *Free Radic. Res.* 25:221–227.

70. Tadolini, B., L. Cabrini, …, G. Hakim. 1997. Iron (III) stimulation of lipid hydroperoxide-dependent lipid peroxidation. *Free Radic. Res.* 27:563–576.

71. Mozuraityte, R., T. Rustad, and I. Storrø. 2008. The role of iron in peroxidation of polyunsaturated fatty acids in liposomes. *J. Agric. Food Chem.* 56:537–543.

72. Tang, L., Y. Zhang, …, X. Shen. 2000. The mechanism of Fe^{2+}-initiated lipid peroxidation in liposomes: the dual function of ferrous ions, the roles of the pre-existing lipid peroxides and the lipid peroxyl radical. *Biochem. J.* 352:27–36.

73. Schneider, C. 2009. An update on products and mechanisms of lipid peroxidation. *Mol. Nutr. Food Res.* 53:315–321.

74. Nimse, S. B., and D. Pal. 2015. Free radicals, natural antioxidants, and their reaction mechanisms. *RSC Adv.* 5:27986–28006.

Biophysical Journal, Volume *112*

Supplemental Information

Antioxidant and Membrane Binding Properties of Serotonin Protect Lipids from Oxidation

Slim Azouzi, Hubert Santuz, Sandrine Morandat, Catia Pereira, Francine Côté, Olivier Hermine, Karim El Kirat, Yves Colin, Caroline Le Van Kim, Catherine Etchebest, and Pascal Amireault

Supporting Material

Antioxidant and Membrane Binding Properties of Serotonin Protect Lipids from Oxidation

Slim Azouzi[1,‡], Hubert Santuz[1,‡], Sandrine Morandat[2], Catia Pereira[1], Francine Côté[3], Olivier Hermine[3], Karim El Kirat[4], Yves Colin[1], Caroline Le Van Kim[1], Catherine Etchebest[1,], and Pascal Amireault[1,3,*].*

1- Université Sorbonne Paris Cité, Université Paris Diderot, INSERM, Unité Biologie Intégrée du Globule Rouge UMR-S1134, Institut National de la Transfusion Sanguine, Laboratoire d'Excellence GR-Ex, Paris, France

2- Sorbonne universités, Université de technologie de Compiègne, CNRS, Laboratoire de Génie Enzymatique et Cellulaire FRE 3580, Centre de recherche Royallieu, Compiègne, France.

3- Université Sorbonne Paris Cité, Université Paris Descartes, INSERM, CNRS, Laboratory of cellular and molecular mechanisms of hematological disorders and therapeutic implications U1163, Institut Imagine, Laboratoire d'Excellence GR-Ex, Paris, France

4- Sorbonne universités, Université de technologie de Compiègne, CNRS, Laboratoire de BioMécanique et BioIngénierie UMR 7338, Centre de recherche Royallieu, Compiègne cedex, France.

Initiation:
$LH + R^{\bullet} \rightarrow L^{\bullet} + RH$ (1)
$L^{\bullet} + O_2 \rightarrow LOO^{\bullet}$ (2)
Propagation;
$LOO^{\bullet} + LH \rightarrow LOOH + L^{\bullet}$ (3)
New chain reaction:
$LOOH \rightarrow LO^{\bullet} + LOO^{\bullet} + RCHO$ (4)
Termination:
$2\,LOO^{\bullet} \rightarrow LOO - OOL$ (5)

Fenton Initiation:
$Fe^{2+} + H_2O_2 \rightarrow Fe^{3+} + OH^{-} + OH^{\bullet}$ (6)
$OH^{\bullet} + LH \rightarrow H_2O + L^{\bullet}$ (7)
AAPH Initiation:
$R - N{=}N - R \rightarrow 2N + 2R^{\bullet}$ (8)
$R^{\bullet} + O_2 + LH \rightarrow ROOH + LOO^{\bullet}$ (9)

Redox cycling of Iron:
$Fe^{3+} + LOOH \rightarrow Fe^{2+} + LOO^{\bullet} + H^{+}$ (10)
$Fe^{2+} + LOOH \rightarrow Fe^{3+} + LO^{\bullet} + OH^{-}$ (11)

Scheme S1: Reactions of oxidation

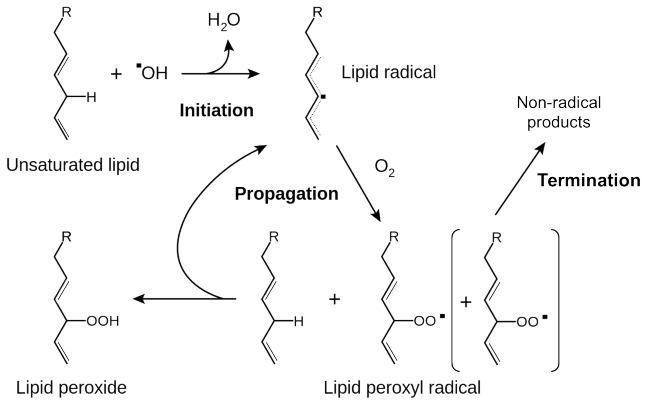

Figure S1: Mechanisms of peroxidation

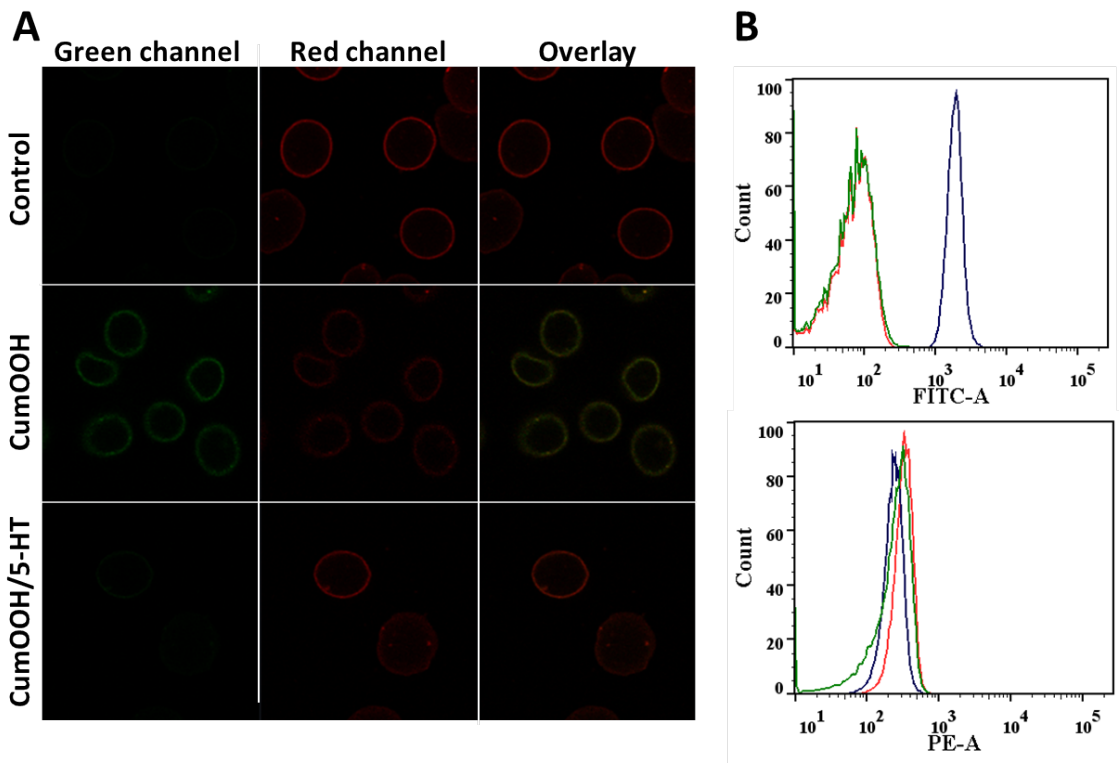

Figure S2: Detection of CumOOH-induced oxidation of BODIPY 581/591 C11 in RBCs using confocal microscopy and flow cytometry. (**A**) Typical fluorescence images obtained from the red and green channels of BODIPY 581/591 C11-labeled RBCs, incubated 2h at room temperature with 150 µM CumOOH or with 150 µM CumOOH/50 µM 5-HT. (**B**) The green and red fluorescence intensities associated with each samples were analyzed by flow cytometry. Fluorescence intensities are shown for untreated samples (red), CumOOH treatment (blue), and CumOOH/5-HT treatment (green). Upon reaction with reactive oxygen species, the red fluorescence of BODIPY 581/591 shifts to green.

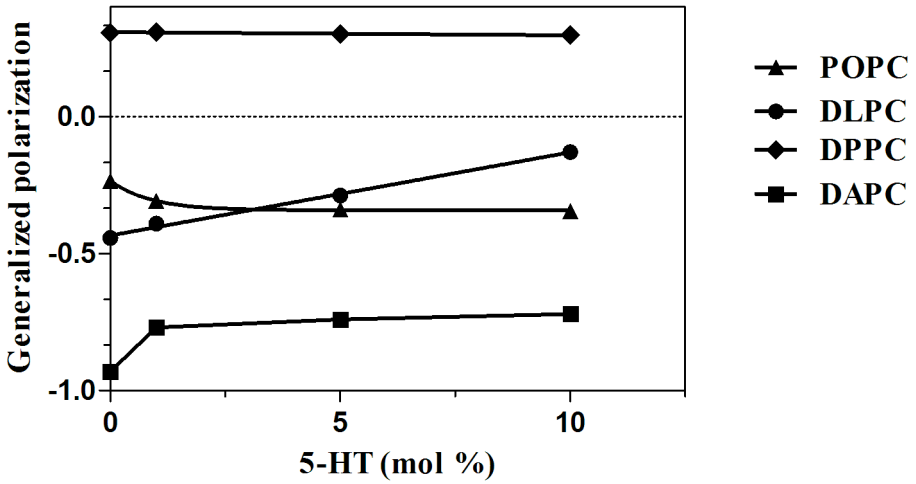

Figure S3: Generalized polarization (GP) of the Laurdan fluorescent probe was plotted as a function of 5-HT content in DAPC, DPPC, DLPC or POPC SUVs at 37°C.

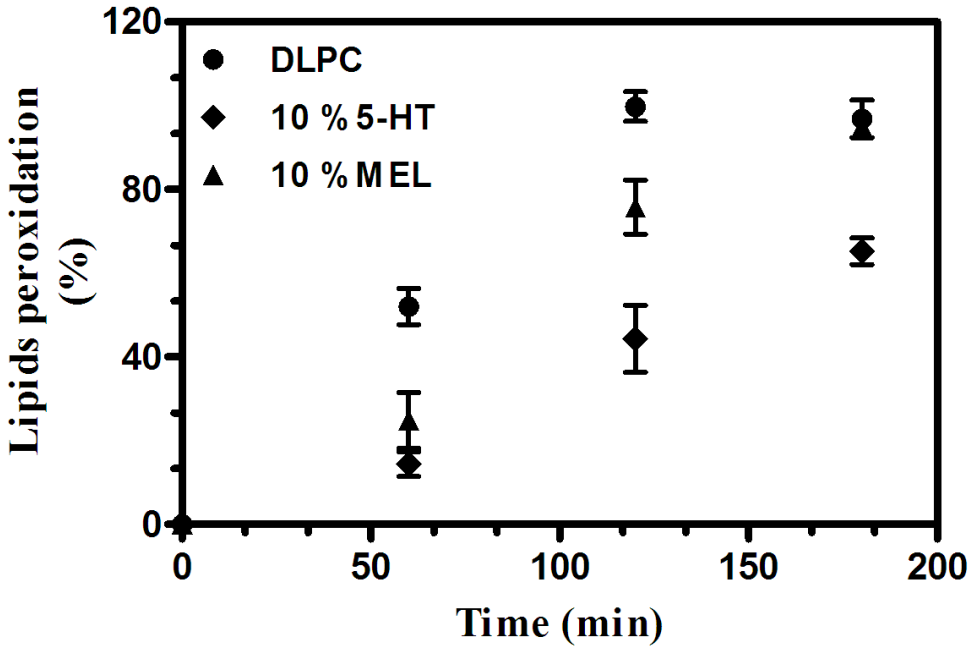

Figure S4: Kinetics of DLPC peroxidation with AAPH measured at 234 nm.

	% of 5-HT (mol)			
	0	1	5	10
DPPC	**55 ± 3 nm**	**49 ± 2 nm**	**50 ± 4 nm**	**47 ± 7 nm**
POPC	**51 ± 4 nm**	**45 ± 3 nm**	**46 ± 6 nm**	**54 ± 4 nm**
DLPC	**49 ± 3 nm**	**55 ± 1 nm**	**56 ± 4 nm**	**52 ± 8 nm**
DAPC	**67 ± 8 nm**	**62 ± 6 nm**	**68 ± 3 nm**	**57 ± 6 nm**

Table S1: The diameters of the different SUVs measured by Dynamic Light Scattering (DLS).

Systems	OH		Amine	
	Water	**Lipid**	**Water**	**Lipid**
POPC	**1.85 ± 0.04**	**0.40 ± 0.01**	**1.64 ± 0.05**	**1.30 ± 0.05**
DLPC	**1.87 ± 0.02**	**0.37 ± 0.01**	**1.73 ± 0.05**	**1.21 ± 0.05**
DAPC	**1.86 ± 0.05**	**0.39 ± 0.02**	**1.76 ± 0.20**	**1.18 ± 0.22**

Table S2: Average number of H-bonds for each system between Amine OH group of 5-HT and water or lipid molecules. The statistical errors were obtained using the block-averaging method. The values agree fairly well those reported by Wood et al (1) for the interactions with lipids (1.611 for the Amine and 0.290 for OH). For water, the values obtained are higher (1.64 comparted to 1.045 for the amine and 1.85 compared to 0.725 for the OH part). This could be explained by a longer time spent by 5-HT in water during our simulations.

	Thickness (nm)	A_L (nm²)
POPC	**3.95 ± 0.06**	**0.62 ± 0.01**
DLPC	**3.80 ± 0.07**	**0.67 ± 0.01**
DAPC	**3.69 ± 0.07**	**0.74 ± 0.02**
DLPC/Z,E-13-HPd	**3.72 ± 0.06**	**0.69 ± 0.01**
DLPC/Z,E-9-Pl$^{\bullet}$	**3.76 ± 0.06**	**0.68 ± 0.01**
DLPC/Z,E-13-Pl$^{\bullet}$	**3.79 ± 0.06**	**0.68 ± 0.01**

Table S3: Properties of pure bilayer membranes. The thickness was defined as the Phosphate-Phosphate distance. The area per lipid (A_L) was calculated by dividing the box area in the dimension parallel to the bilayer plane by the number of lipids in each leaflet.

	HeadGroup	Glycerol	Aliphatic Chains
DLPC	**41.2**	**22.4**	**36.4**
DLPC/Z,E-13-HPd	**37.3**	**21.9**	**40.8**
DLPC/Z,E-9-Pl$^{\bullet}$	**42.62**	**22.49**	**34.94**
DLPC/Z,E-13-Pl$^{\bullet}$	**40.66**	**22.25**	**37.11**

Table S4: Type of contacts (in %) between 5-HT and membrane. A Contact is defined if the distance between any atoms of the lipids and the center of mass of 5-HT lipid is inferior to 0.6 nm.

Text S1: Protocol of Potential of Mean Force

Umbrella sampling simulations were performed for serotonin crossing membrane of three different compositions, i.e pure POPC, pure DLPC and pure DAPC. Software version, forcefield parameters and simulations conditions were the same as used in the standard molecular dynamics simulations described in Material and Methods section. The starting frames for the umbrella simulations were taken from the last frame of the pure bilayers simulations. The system was composed of 128 phospholipids and around 10 000 water molecules. To construct the configurations, the center of mass (COM) of 5-HT were placing at different z-position separated by 1A with a range between -39 Å and 39 Å. To enhance sampling, 2 molecules of 5-HT were added at different z positions, keeping a distance of 39 Å between them. In each window of umbrella sampling, the simulation was carried out for 10 ns by applying a force constant of 1000 kJ/mol/nm² based on the COM of the 5-HT molecules. For the positions located within the membrane interface (between 12 Å and 26 Å and between -12 Å and -26 Å), the simulation time for sampling was lengthened up to 50 ns.

The PMFs were computed using the weighted histogram analysis method (WHAM) (2) as implemented in the g_wham software (3). Statistical errors were calculated using bootstrap analysis.

References

1. Wood, I., M.F. Martini, and M. Pickholz. 2013. Similarities and differences of serotonin and its precursors in their interactions with model membranes studied by molecular dynamics simulation. J. Mol. Struct. 1045: 124–130.
2. Kumar, S., J.M. Rosenberg, D. Bouzida, R.H. Swendsen, and P.A. Kollman. 1992. THE weighted histogram analysis method for free-energy calculations on biomolecules. I. The method. J. Comput. Chem. 13: 1011–1021.
3. Hub, J.S., B.L. de Groot, and D. van der Spoel. 2010. g_wham—A Free Weighted Histogram Analysis Implementation Including Robust Error and Autocorrelation Estimates. J. Chem. Theory Comput. 6: 3713–3720.